A Method for Estimation of Atmospheric Water Vapor Profiles by Microwave Radiometry

P. W. ROSENKRANZ, M. J. KOMICHAK AND D. H. STAELIN

Research Laboratory of Electronics, Massachusetts Institute of Technology, Cambridge 02139

(Manuscript received 18 August 1981, in final form 2 April 1982)

ABSTRACT

Simultaneous measurements of microwave emission from the earth, in the oxygen band near 60 GHz and the water vapor line near 183 GHz, permit inference of atmospheric temperature as a function of two variables: pressure and water vapor burden (integrated water vapor content above any level). Combination of these two profiles yields a profile of water vapor burden versus pressure. Occasional singularities in these retrievals can readily be identified and excluded. Numerical simulations have been made, using temperature and water vapor profiles from subtropical and midlatitude radiosonde stations, and assuming surface reflectivities typical of either land or ocean. Over a land surface, the residual rms errors in estimated water vapor burden profile between 300 and 1000 mb, range from 23 to 43% of the *a priori* standard deviation of water vapor burden for the corresponding climate. The relative humidity profile was also estimated with rms errors ranging from 4 to 17% of saturation. Over a seawater surface, using three additional channels at 18.5, 22.2 and 31.7 GHz, the corresponding results are 3–46% of *a priori* standard deviation for water vapor burden and 4–15% rms error for relative humidity.

1. Introduction

The ability of microwave radiation to penetrate nonprecipitating clouds, especially cirrus, recommends the use of those frequencies for remote sensing of the atmosphere (Staelin *et al.*, 1977). Water vapor has two lines below 300 GHz, a weak line at 22.2 GHz and a strong line at 183.3 GHz. Until now, satellite microwave radiometers have only made use of the 22 GHz line, which is not opaque in the atmosphere, and, therefore, have been able to estimate only the total water vapor burden, rather than a profile, and only over the ocean, which provides a radiometrically cold background (Staelin *et al.*, 1976). The 183 GHz line is sufficiently strong that, by observation with a radiometer at several frequencies at various displacements from line center, one would measure thermal emission from different levels in the absorbing medium, probing more deeply with increasing distance in frequency from line center. This principle has been demonstrated using the oxygen band near 60 GHz to estimate atmospheric temperature profiles (Waters *et al.*, 1975). Measurements near the strong water vapor line would respond to variation of temperature as a function of opacity due to the atmospheric water vapor.

2. Line formation and weighting functions

The intensity of thermal microwave emission from the atmosphere at a specified frequency ν and direction is characterized by a brightness temperature $T_{B\nu}$. For an atmosphere with no scattering, above a flat surface with reflectivity R,

$$T_{B\nu} = \exp(-\tau_{\text{surf}})[T_{\text{surf}}(1 - R) + RT^{\downarrow}_{B\nu}] + \int_{\exp(-\tau_{\text{surf}})}^{1} T(\tau)d\exp(-\tau), \quad (1)$$

where T is atmospheric temperature, T_{surf} is the temperature of the surface, $T^{\downarrow}_{B\nu}$ is the sky brightness temperature at the surface, and τ is the opacity from the top of the atmosphere down to a point a:

$$\tau = \int_a^{\infty} \rho(s)k[f(\nu, P), T]ds, \quad (2)$$

where ds is a differential element along the path of the radiation, $\rho(s)$ is the density of the absorbing gas and $k[f(\nu, P), T]$ is the absorption coefficient per unit density, which in turn is a function of the line shape factor $f(\nu, P)$ where P is the total pressure, and temperature T. τ_{surf} is the opacity to the surface.

Eq. (1) is based on a linearization of the Planck function of intensity versus kinetic temperature. Even at the high frequencies with which we are concerned here, the Planck function is sufficiently linear over the range of temperatures occurring in the atmosphere that, after a radiometer is calibrated with blackbody sources at known temperatures, (1) can be employed with errors of less than a few hundredths of a Kelvin.

Let us consider for now a black surface ($R = 0$).

0021-8952/82/091364-07$05.75

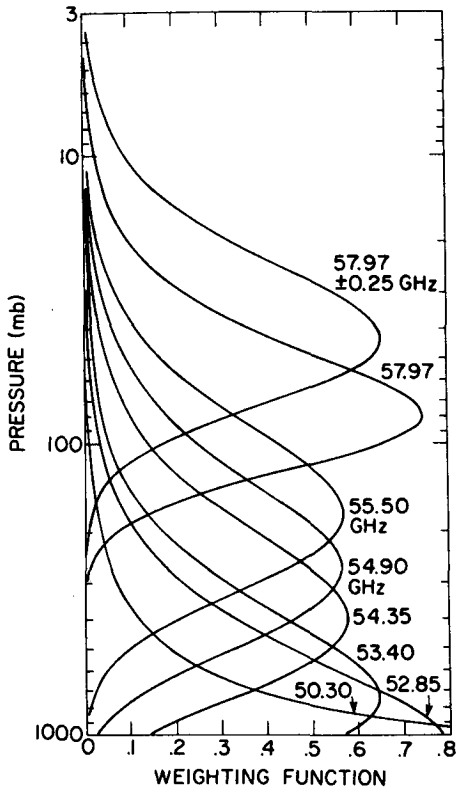

FIG. 1. Temperature weighting functions in the oxygen band for vertical incidence.

For the purpose of understanding what the brightness temperature measurement represents (as distinguished from actual computation of $T_{B\nu}$) it is useful to define a temperature weighting function $W(s)$ where

$$W(s)ds = d\exp(-\tau), \tag{3}$$

so that substitution of (3) into (1) gives a linear integral equation with $W(s)$ multiplying temperature $T(s)$ inside the integral. The substitution (3) is most useful when s is measured in such a way that $W(s)$ is nearly independent of variables other than s and frequency. In the case of frequencies near the oxygen band, the primary absorbing constituent in the atmosphere is uniformly mixed, so both total pressure and its logarithm are closely coupled to opacity τ and either is a good variable with which to identify s. In the case of water vapor, τ depends on both the density of water vapor and the total pressure (which influences line width), but in the atmosphere the water vapor density varies over two or three orders of magnitude in a range of pressures from 250 to 1000 mb. If the slower variations of P and T along the path of the radiation are neglected, then τ becomes proportional to water vapor burden, which is the integrated mass of water vapor above a given level. This variable or its logarithm are therefore good variables with which to identify s. The use of logarithmic measures for s produces temperature weighting functions with a high degree of symmetry, as illustrated in Fig. 1 for frequencies in the oxygen band and Fig. 2 for frequencies near the water vapor line. These weighting functions were computed for a tropical model atmosphere. We have also computed weighting functions for a standard midlatitude atmosphere. They look very much like Fig. 2, differing only by typically being shifted upward by a factor of ~0.8 in water vapor burden, which shows that water vapor density is indeed the most significant variable in (2).

It is also possible to define weighting functions for water vapor density, as shown by Schaerer and Wilheit (1979); but these water vapor weighting functions depend strongly on the water vapor profile and the problem then becomes nonlinear. Our purpose is to retain the linearity of (1) as far as possible.

3. Inversion of the radiometric measurements

Having (1) in a linear form justifies the use of a linear estimation algorithm for temperature. Linear regression (Deutsch, 1965) is widely used in remote sensing because of its simplicity and robustness in the presence of noise. Let $\mathbf{y}$ be the vector of observed brightness temperatures and $\hat{\mathbf{x}}$ be the estimate of the atmospheric temperature vector $\mathbf{x}$. Then

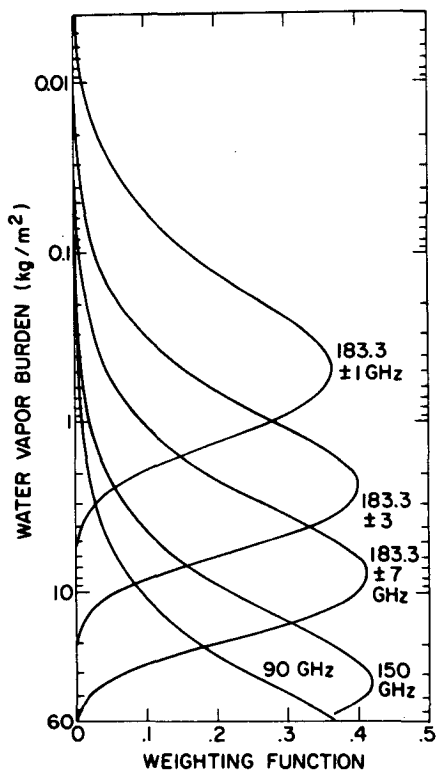

FIG. 2. Temperature weighting functions near the 183 GHz water vapor line.

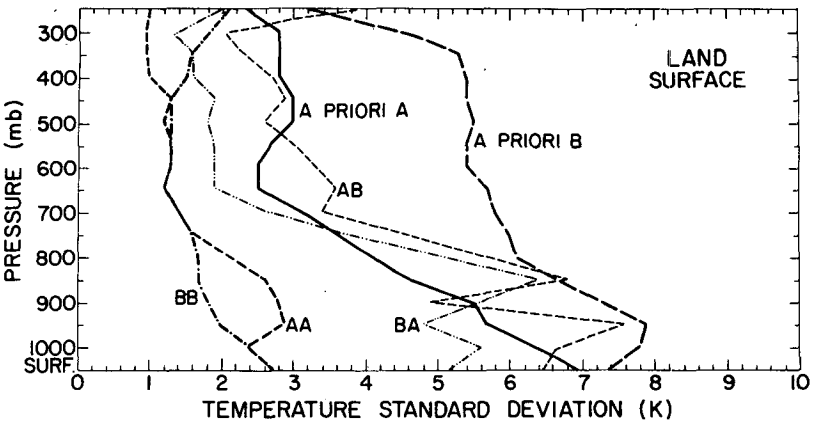

FIG. 3. Residual temperature profile retrieval errors from simulations in which two sets of radiosonde temperature profiles were regressed against brightness temperatures at frequencies of Figs. 1 and 2. The surface was assumed to be land. AB: set A (subtropical) used to generate covariance matrices, set B (midlatitude) used for testing. BA: set B used for generating covariances, set A for testing. AA: set A used for both generation and testing. BB: set B used for both generation and testing. *A priori* A and *a priori* B: standard deviations of sets A and B.

$$\hat{\mathbf{x}} = \mathbf{R}_{xy}\mathbf{R}_{yy}^{-1}(\mathbf{y} - \langle \mathbf{y} \rangle) + \langle \mathbf{x} \rangle, \tag{4}$$

where angle brackets denote mean values and $\mathbf{R}_{xy}$ and $\mathbf{R}_{yy}$ are respectively covariance matrices of x and y and y with itself. These statistics were computed from brightness temperatures simulated by integration of (1) using finite-difference methods for two different sets of radiosonde data: set A consisted of 17 soundings from San Juan, Puerto Rico and 36 from Pt. Mugu, CA; set B consisted of 100 soundings from Peoria, IL and 53 from Ocean Station P. The Peoria soundings were from the months of June–September in 1966 and 1967 and the others were all from June 1970. In computing $\mathbf{R}_{yy}$ it was assumed that the measured brightness temperatures would contain independent errors of 0.5 K rms on the oxygen band channels and 0.6 K rms on the water vapor channels. With real data it would be necessary to distinguish between brightness temperature and antenna temperature, and make corrections to the latter to obtain the former; but we shall not address this problem here.

The first numerical experiment was designed to simulate remote sensing over a land surface. When the brightness temperatures were computed, it was assumed that the surface had an average reflectivity of 0.1, with a standard deviation about the mean of 0.05 at all frequencies. The random components of reflectivity, at frequencies separated approximately by half an octave (e.g., 90 and 150 GHz), were assumed to be correlated with a coefficient of 0.99. These values are typical for earth and vegetation. More widely separated frequencies were correspondingly less correlated. Clouds were not included in these simulations, but a brief discussion of possible errors from clouds is given below.

Figs. 3 and 4 contain plots of the residual errors

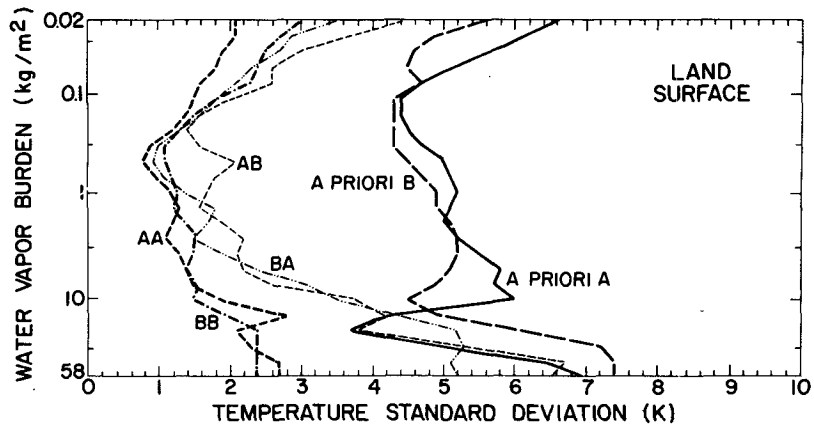

FIG. 4. Residual temperature profile retrieval errors as in Fig. 3, but with temperature a function of water vapor burden.

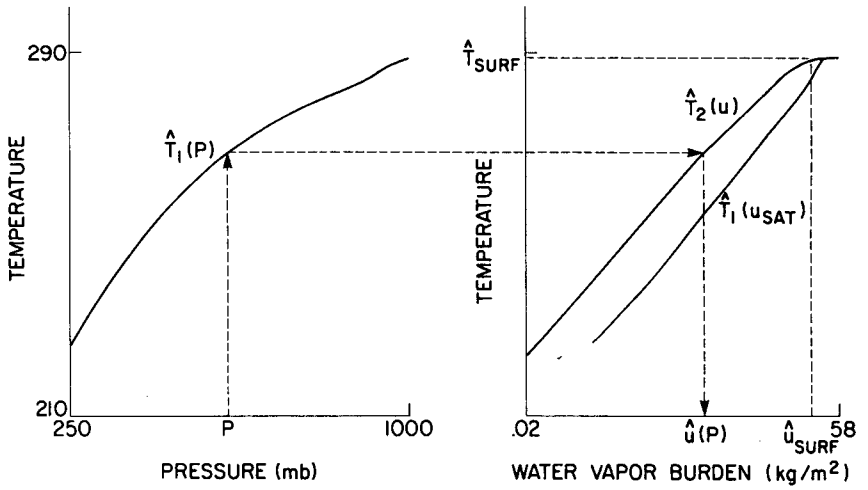

FIG. 5. Illustration of the method of obtaining the preliminary estimate of water vapor burden u as a function of pressure P, given two estimated temperature profiles. The temperature and pressure axes are linear, and the water vapor axis is logarithmic.

obtained from simulations in which the temperature profile, as a function of pressure and water vapor burden, respectively, was estimated from brightness temperatures computed at the frequencies listed in Figs. 1 and 2. Also plotted are the *a priori* standard deviations of the two sets of statistics. When the coefficients in the regression are derived for one climate and applied to data from the other climate, as is the case for the curves labeled AB and BA, the errors give an indication of the extent to which the results are dependent on statistical information. Normally the coefficients and data would be from similar climates.

Although it is not a standard practice to plot temperature as a function of water vapor, the utility of such a function lies in interpolation of the temperature versus water vapor burden profile to the values of temperatures at standard pressures estimated from the oxygen band. One thereby obtains a preliminary estimate of the water vapor burden at each of the standard pressures. This procedure is shown schematically in Fig. 5, where $\hat{T}_1(P)$ is temperature estimated for 16 fixed pressure levels between 250 and 1000 mb and $\hat{T}_2(u)$ is temperature estimated for 24 fixed values of water vapor burden between 0.02 and 58 kg m^{-2}. (The two profiles $\hat{T}_1(P)$ and $\hat{T}_2(u)$ drawn in the figure are actually mean profiles for radiosonde set *B*.)

For u larger than the surface water vapor burden, $\hat{T}_2(u)$ is approximately equal to the surface temperature. We defined an isothermal region to consist of temperature variations of ≤ 1 K. The smallest value of u within the isothermal region at the right side of Fig. 5 was assumed to be the surface water vapor burden. If $\hat{T}_{surf} > \hat{T}_1$ (1000 mb), this assumption is sufficient to permit the construction of $\hat{u}(P)$. However, if $\hat{T}_1$ (1000 mb) $> \hat{T}_{surf}$, let u_1 be the value of u corresponding to the highest $\hat{T}_1(P)$ less than $\hat{T}_{surf}$, and let n be the number of pressure levels for which $\hat{T}_1(P) > \hat{T}_{surf}$. Then the interval between $\hat{u}_{surf}$ and u_1 was (arbitrarily) divided equally into n segments, and the resulting values of u were assigned to the corresponding values of P. The latter situation occurred in almost all of the profiles in our two data sets, which indicates that $\hat{T}_{surf}$ is being slightly underestimated.

A constraint can be placed on the profile $\hat{T}_2(u)$ if the water vapor burden at any given level is not allowed to exceed the values which it would have, if the atmosphere were saturated at all lower pressures. This value will be denoted by u_{sat} and was estimated from $\hat{T}_1(P)$ [which is our best estimate of $T(P)$] by a trapezoidal integration:

$$u_{sat}(P) = \sum_{P' \leq P} q_{sat}(\hat{T}_1, P')\Delta P/g, \qquad (5)$$

where g is the acceleration of gravity and q_{sat} is the saturation value of specific humidity (density of water vapor divided by total air density) which is computable by well-known formulas. The value of ΔP was 50 mb, except at the lowest pressure level of 250 mb, where we set $\Delta P = 75$ mb to account for all vapor at lower pressures, and at $P' = P$, where $\Delta P = 25$ mb. If the temperature from profile 1 ($\hat{T}_1$) is plotted on the right side of Fig. 5 as a function of u_{sat}, as shown, then profile 2 ($\hat{T}_2$) should lie to the left of it at all points. $\hat{T}_2(u)$ could in fact cross over $\hat{T}_1(u_{sat})$ due to normal estimate errors or, with real data, due to the presence of an opaque cloud in the atmosphere. Such a cloud would cause the estimated temperature profile $\hat{T}_2(u)$ to level off at approximately the temperature of the level at which the opacity reached unity, instead of at T_{surf}. Profile 1 would be similarly affected except that the oxygen band channels would see deeper into

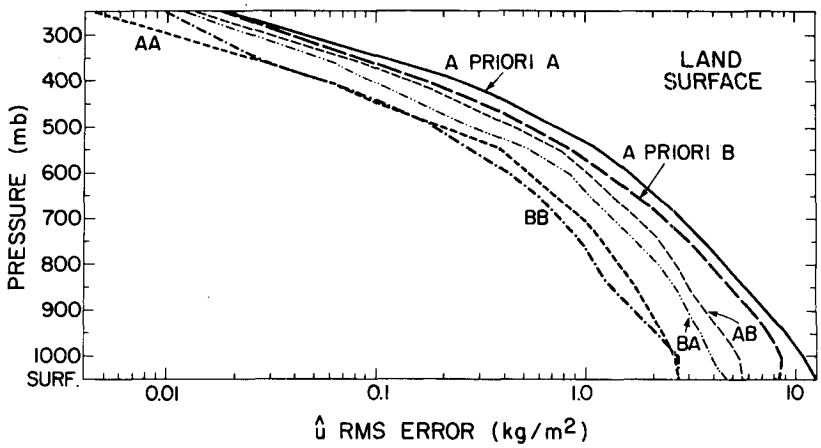

FIG. 6. Residual errors in estimated water vapor burden, over land. AB, BA, AA, BB, *a priori* A and *a priori* B have the same meaning as in Fig. 3.

the cloud and $\hat{T}_1(P)$ would therefore probably reach a higher temperature. In either case, values of $\hat{u} > u_{sat}$ would be replaced by u_{sat}, or if $\hat{u} - u_{sat}$ exceeded a preset positive value, the profile might be rejected as excessively cloud-contaminated.

This procedure of matching the two temperature profiles gives an unambiguous result if the estimated temperature increases monotonically with pressure. Otherwise, there is more than one possible solution for $\hat{u}(P)$. Even when the procedure produced an unambiguous result, we found that its accuracy could be improved by another step of linear regression, in which the preliminary profile of water vapor burden sampled at 100 mb intervals was concatenated with the vector of 90–183 GHz brightness temperatures and the resulting vector used as the predictor [y in Eq. (4)] and $\hat{\mathbf{x}}$ was the final estimate of water vapor burden. When either $\hat{T}_1(P)$ or $\hat{T}_2(u)$ were nonmonotonic, which was the case with 42% of the subtropical profiles and 25% of the midlatitude profiles, we used the brightness temperatures alone as the predictor. The rms errors in the final estimate of water vapor burden are plotted in Fig. 6.

Because the specific humidity in the atmosphere tends to be a rapidly increasing function of pressure, the ratio u/u_{sat} is highly correlated with the relative humidity. Having estimated $\hat{u}$ as a function of pressure, and having calculated u_{sat} from $\hat{T}_1(P)$, we can profitably use the statistical method again to estimate relative humidity as a function of pressure. Referring to Eq. (4), x is identified with relative humidity and y is a vector formed by linking the 90–183 GHz brightness temperatures with the vector of $\hat{u}/u_{sat}$ values. The residual errors in estimation of relative humidity are plotted in Fig. 7. Also plotted for comparison, and labeled "AA linear" and "BB linear," are residual errors obtained without using $\hat{u}/u_{sat}$, i.e., a straightforward linear regression of relative humidity on all brightness temperatures. Note that use of the nonlinear procedures described here provides a

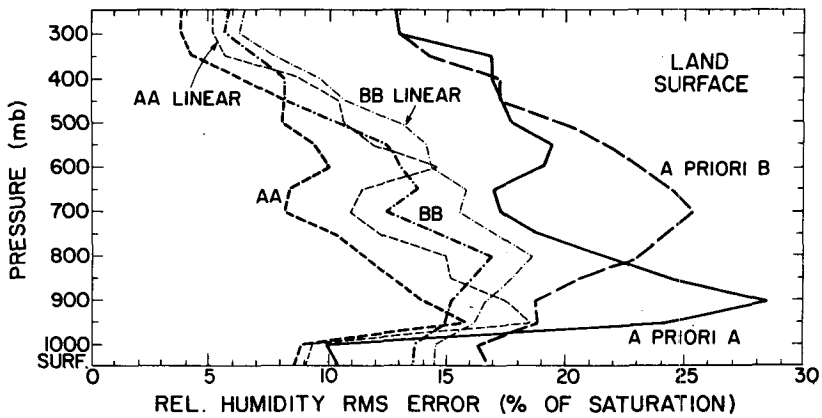

FIG. 7. Residual errors in estimated relative humidity, over land. AA, BB, *a priori* A and *a priori* B have the same meaning as in Fig. 3. AA linear and BB linear are the rms errors obtained using only linear regression techniques.

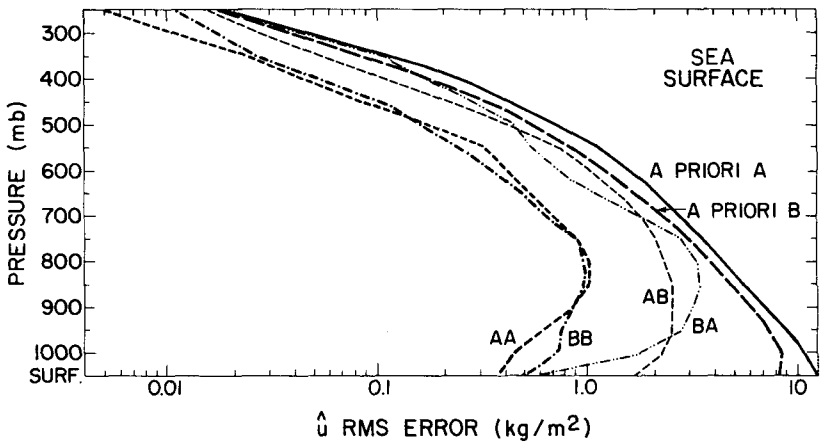

FIG. 8. Residual errors in estimated water vapor burden over a smooth ocean surface. AB, BA, AA, BB, *a priori* A and *a priori* B have the same meaning as in Fig. 3.

factor of ~20% improvement in rms error (i.e., 3% of saturation) over traditional linear regression techniques.

In the second numerical experiment, we simulated brightness temperatures as they would be observed over a smooth ocean surface. The oceans have appreciably higher reflectivity (~0.3 near 183 GHz) than land. Thus, in the more transparent water vapor channels at 90 and 150 GHz, the brightness temperature $T_{B\nu}$ contains a component of emission which propagates downward from the atmosphere and is reflected from the surface:

$$T_{B\nu} = \int_{\exp(-\tau_{\text{surf}})}^{1} T(u)d\exp[-\tau(u)] + \exp(-\tau_{\text{surf}})\{T_{\text{surf}}(1-R) + R\int_{\exp(-\tau_{\text{surf}})}^{1} T(u)d\exp[-\tau(u,u_{\text{surf}})]\}, \quad (6)$$

where R is the reflectivity of the surface, $\tau(u, u_{\text{surf}})$ is the opacity from the surface to level u and $\tau(u)$ is the opacity from the top of the atmosphere to level u, given by (2). The strength of this reflected component, the third term, depends on τ_{surf}, a function of the surface water vapor burden, which is variable. In order to use the linear regression Eq. (4) to relate the temperatures (x) at fixed values of atmospheric water vapor burden u to brightness temperatures (y), we must define temperature for all values of u in such a way that linearity is preserved; or in other words, as though the atmosphere were infinitely deep. Eq. (6) can be rewritten in such a form since T_{surf} is not a function of u:

$$T_{B\nu} = \int_0^{\tau_{\text{surf}}} T(u)\exp[-\tau(u)]d\tau(u) + (1-R)\int_{\tau_{\text{surf}}}^{\infty} T_{\text{surf}}\exp(-\tau)d\tau + R\int_0^{\tau_{\text{surf}}} T(u)\exp[-\tau_{\text{surf}} - \tau(u,u_{\text{surf}})]d\tau(u,u_{\text{surf}}) \quad (7)$$

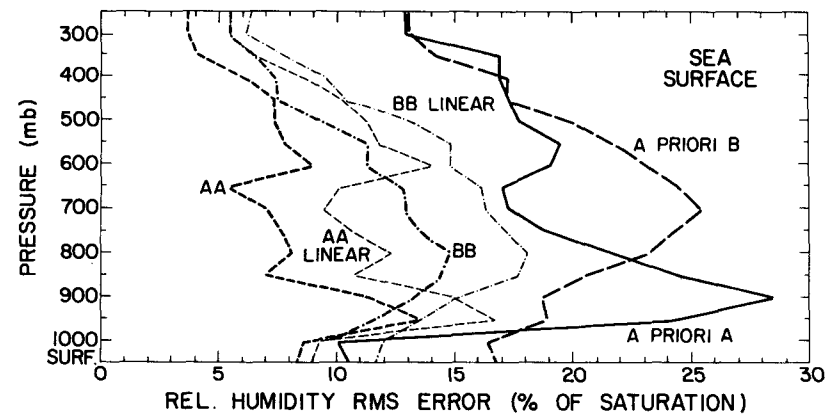

FIG. 9. Residual errors in estimated relative humidity over a smooth ocean surface. AA, BB, *a priori* A, *a priori* B, AA linear, and BB linear have the same meaning as in Figs. 3 and 7.

or

$$T_{B\nu} = \int_0^{\tau_{surf}} T(u) \exp[-\tau(u)] d\tau(u) + (1 - R) \int_{\tau_{surf}}^{\infty} T_{surf} \exp(-\tau) d\tau + R \int_{\tau_{surf}}^{2\tau_{surf}} T(2u_{surf} - u) \exp[-\tau(u)] d\tau(u), \quad (8)$$

where $\tau(u)$ for $u > u_{surf}$ is defined as

$$\tau(u) = \tau_{surf} + \tau(u - u_{surf}), \quad (9)$$

and we make the approximation that $\tau \propto u$. In the case of a black surface ($R = 0$) the brightness temperatures are the same as would be observed from an infinitely deep atmosphere which was isothermal below the surface. A perfectly reflecting surface ($R = 1$) would produce brightness temperatures equal to those which would be observed from an atmosphere whose temperature profile below the surface level was a mirror image of the temperature profile above the surface. Therefore, since brightness temperature is a linear function of R we defined temperature $T(u)$ for $2u_{surf} > u > u_{surf}$ as

$$T(u) = (1 - R)T_{surf} + RT(2u_{surf} - u). \quad (10)$$

The value of R changes slightly with frequency, so we chose R (150 GHz) as the best compromise. Note that (8) and (9) were introduced only to demonstrate the linear relation of the brightness temperature to temperature profile; (6) defines brightness temperature for the purpose of computations.

The data inversion procedure was essentially the same as for land, with the exception of the estimation of surface water vapor burden. This quantity can be estimated accurately over an ocean background using measurements near 22 GHz, as described by Staelin *et al.* (1976). We computed simulated brightness temperatures at 18.5, 22.23 and 31.65 GHz for each sounding in the two sets of statistics and used Eq. (4) to estimate u_{surf} from those three brightness temperatures. Given $\hat{u}_{surf}$ as the starting point, the rest of the preliminary profile of $\hat{u}(P)$ was filled in by combining the $\hat{T}_1(P)$ with the $\hat{T}_2(u)$ profiles as in Fig. 5 for the case of a land surface. In this experiment 47% of the estimated subtropical profiles and none of the midlatitude profiles were nonmonotonic.

Results are shown in Figs. 8 and 9. As expected, the accuracy of the surface water vapor burden is improved, compared to the case of land surfaces. At the upper levels in the atmosphere, the accuracy of the estimates is similar. Again this nonlinear procedure offers significant improvement relative to linear regression techniques, indicated by "AA linear" and "BB linear."

4. Summary and directions for future research

We have simulated the retrieval of water vapor burden and relative humidity profiles from satellite-based radiometric measurements near 60 and 183 GHz. This estimation method could easily be adapted to infrared or ground-based microwave measurements. It involves combination of two temperature profiles obtained from measurements made in the oxygen band and near an opaque water vapor line. In these experiments the rms errors in the relative humidity estimates were reduced 20–24% compared to those obtained with linear regression techniques.

The present simulations do not include the effects of clouds, although the comparison of $\hat{u}$ with u_{sat} provides a way of determining from the data, the presence of an opaque cloud. Detection and correction for semi-transparent clouds and for opaque clouds that only partially fill the antenna beam is a problem on which additional work is required.

Acknowledgment. This research was supported by NASA grant NAG5-10.

REFERENCES

Deutsch, R., 1965: *Estimation Theory.* Prentice-Hall, 269 pp.

Schaerer, G., and T. T. Wilheit, 1979: A passive microwave technique for profiling of atmospheric water vapor. *Radio Sci.*, **14,** 371–375.

Staelin, D. H., K. F. Kunzi, R. L. Pettyjohn, R. K. L. Poon, R. W. Wilcox and J. W. Waters, 1976: Remote sensing of atmospheric water vapor and liquid water with the Nimbus 5 microwave spectrometer. *J. Appl. Meteor.*, **15,** 1204–1214.

——, P. W. Rosenkranz, F. T. Barath, E. J. Johnston and J. W. Waters, 1977: Microwave spectroscopic imagery of the earth. *Science*, **197,** 991–993.

Waters, J. W., K. F. Kunzi, R. L. Pettyjohn, R. K. L. Poon and D. H. Staelin, 1975: Remote sensing of atmospheric temperature profiles with the Nimbus 5 microwave spectrometer. *J. Atmos. Sci.*, **32,** 1953–1969.